On the sealing mechanism of radial lip seals

On the sealing mechanism of radial lip seals

M.J.L. Stakenborg*

The sealing mechanism of radial lip seals is considered in a new light. The influence of temperature is described and the use of the finite element method for studying the seal–shaft contact problem is discussed. Observations of the under-lip contact area using glassfibre optics are presented. The oil–air interface formed on the air side of the seal and the occurrence of cavitation are considered. An attempt is made to determine the pumping action of radial lip seals for a steady-state situation by calculating the pressure drop over the oil–air interface on the air side of the seal.

Keywords: *sealing mechanism, radial lip seals, cavitation, finite elements, contact problem*

Notation

b	Contact width, m
d_1	Diameter shaft, m
d_2	Diameter unloaded seal, m
F_r	Radial contact force, N
F_{r1}	Radial lip force, N
F_{r2}	Radial garter spring force, N
h	Gap height between seal and shaft surface, m
l_i	Distance, m
m_{spr}	Mass of garter spring, kg
M	Torque, N m
p	Pressure, Pa
p_0	Static contact pressure, Pa
q	Heat rate, W
R	Radius of oil-air interface, m
t	Time, s
T	Temperature, °C
α_1	Wetting angle for oil–rubber, rad
α_2	Wetting angle for oil–steel, rad
γ	Surface tension of oil in air, N m
η	Dynamic viscosity, Pa s
λ	Thermal conductivity, W mK^{-1}
ρ_{seal}	Specific mass of seal material (Viton), kg m^{-3}
ω_1	Shaft angular velocity, rad s^{-1}
ω_2	Seal angular velocity, rad s^{-1}
ω_{c1}	Air side cavitation initiation velocity, rad s^{-1}
ω_{c2}	Oil side cavitation initiation velocity, rad s^{-1}

Introduction

Radial lip seals are used in machinery to seal rotating shafts at low pressures and to prevent the penetration of dust, dirt or water from the outside. A standard radial lip seal has a stiff mounting part (synthetic rubber body reinforced with a metallic case) and a flexible part (synthetic rubber seal lip with a metallic garter spring; see Fig 1). A difference in the outer diameter d_1 of the shaft and the inner diameter d_2 of the unloaded seal results in a radial contact force F_r. This contact force F_r is the sum of a force F_{r1} due to elastic deformation of the lip and a force F_{r2} caused by elongation of the garter spring.

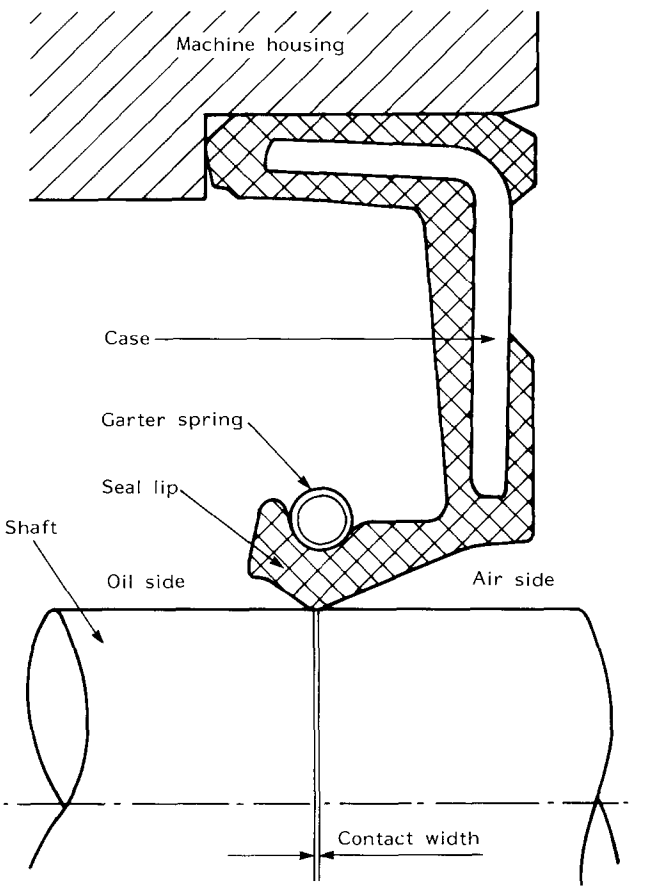

Fig 1 Standard radial lip seal

**Institute for Power Transmissions and Tribology, Eindhoven University of Technology, Postbox 513, 5600 MB Eindhoven, The Netherlands*

 0301-679X/88/060335-06 $3.00

These relatively simple construction elements exhibit a quite remarkable sealing performance and service life. The sealing mechanism of these seals is based on the formation of a thin lubricating and sealing oil film between seal lip and rotating shaft. In the last 30 years intensive research has been performed into the sealing mechanism of these seals. In spite of this effort the sealing mechanism is still poorly understood. In the literature on radial lip seals a number of physical models have been presented for the description of the formation of the lubricating oil film and its sealing properties[1-5,7]. However, these models are not generally accepted by the different investigators. It is clear that the sealing mechanism is based on a complex interaction between seal, oil film and shaft. This tribological system (seal–oil film–shaft) is governed by many variables such as oil viscosity, physical properties of the seal material, shaft diameter, shaft angular velocity, contact force, contact pressure distribution, contact width, surface tension of the oil and temperature.

It was found that the sealing properties of these seals are based on a pumping action. Proper functioning seals are able to pump oil from the air side to the oil side of the seal. This pumping action is determined by the contact conditions.

Contact conditions

The contact force F_r, the contact width b and the contact pressure distribution $p_0(x)$ form boundary conditions for the lubrication mechanism and pumping action. Modelling the lubrication mechanism and pumping action is complicated by the fact that the boundary conditions vary as a function of the service conditions. Due to viscous shear heat dissipation in the thin interfacial oil film between seal and shaft a heat rate q is generated. This results in an increase in the average interfacial temperature T. An increase in shaft angular velocity ω_1 causes an increase in q and thus an increase in T. An increase in T does not only decrease the viscosity η of the oil film, it also changes the boundary conditions because F_r, b and $p_0(x)$ vary with T. Fig 2 shows for instance a considerable decrease in contact width under the influence of temperature. The average interfacial film temperature T resulting from a certain q is determined by the heat balance in the complete machine. Depending on the heat transfer properties of the shaft and depending on the existence of additional heat sources such as bearings, relatively high average film temperatures (ie $T > 150°C$) may occur. Differences in heat transfer properties also explain why experimental torque measurements on identical seals may give different results for different test rigs, and why two identical seals in two different locations in the same construction may exhibit considerable differences in sealing performance and service life.

Experimental determination of the functions $F_r = F_r(T)$, $b = b(T)$ and $p_0(x) = p_0(x, T)$ is difficult because of the broad temperature range occurring in practice ($-40 < T < +150°C$) and because of the small dimensions of the contact width b ($0.05 < b < 0.5$ mm). Here the finite element method can be of great help.

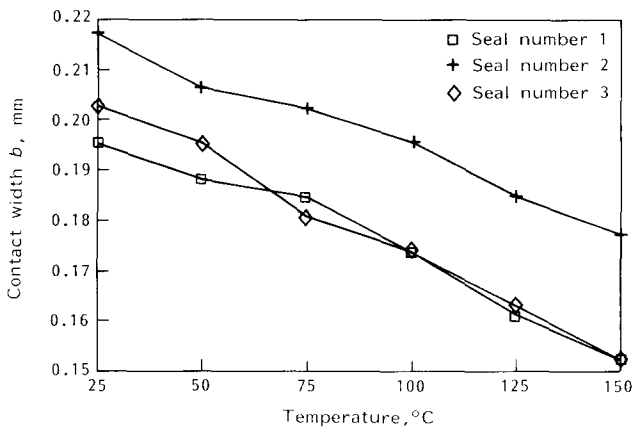

Fig 2 Contact width b *as a function of the seal temperature* T *for three radial lip seals (Viton) of the same type with garter spring (for* $\omega_1 = \omega_2 = 0$*)*

The finite element method

The finite element method (FEM) is a numerical tool which can be useful when studying the seal–shaft contact conditions (Fig 3). An important complication in the use of the FEM is the appropriate characterization of the mechanical properties of the synthetic rubber seal material. The reliability of the numerical output of FEM calculations depends on the accuracy of the constitutive law, which describes the mechanical material behaviour in terms of stress– strain–temperature relations. The parameters from constitutive laws vary for each synthetic rubber and have to be determined experimentally, for example by tensile tests on rubber specimens. These synthetic rubbers exhibit a rather complex material behaviour compared with that of materials like steel. Rubbers exhibit a non-linear thermo-visco-elastic behaviour. Non-linear refers to the relationship between stresses and strains; the stiffness of rubber is not constant, but a function of the strain. Thermo-visco-elastic indicates that the mechanical material behaviour is a function of temperature, and that also viscose or time effects, such as creep and relaxation, occur. Thus, as input to the FEM calculations, a material characterization or constitutive law containing the parameters σ (stress), ε (strain), T (temperature) and t (time) is required.

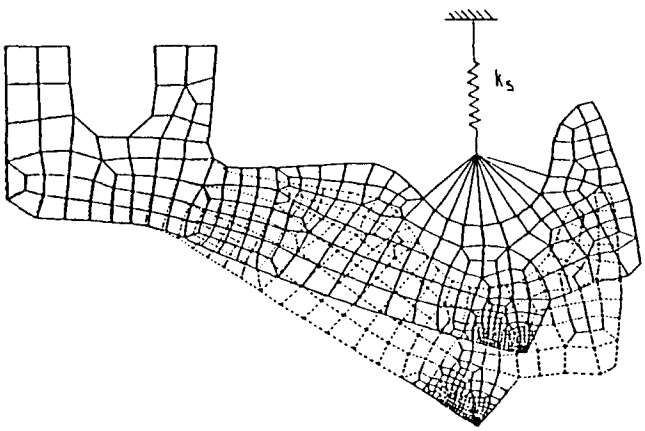

Fig 3 Finite mesh used for calculations on radial lip seal in undeformed and deformed conditions. The garter spring was taken into account by introducing spring element k_s

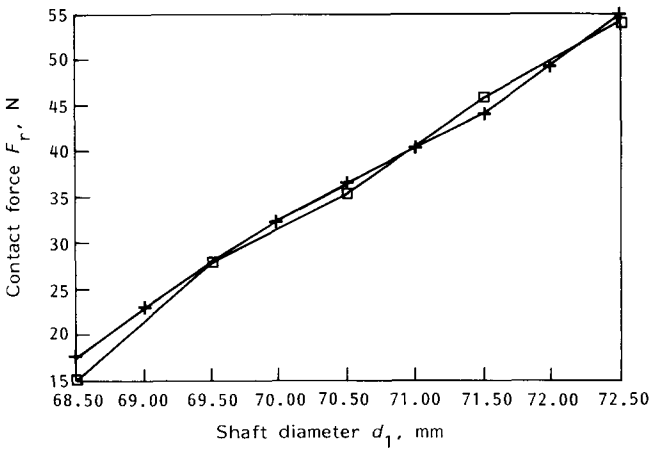

Fig 4 Contact force $F_r = F_r(d_1)$ *after* t = *24 h at temperature* T = 20°C, *calculated with finite element model and measured with split shaft device, for a radial lip seal of Viton, including a garter spring. Nominal shaft diameter* $d_1 = 0.07$ *m*

Fig 4 shows the measured and calculated values of F_r for a Viton-rubber lip seal for different shaft diameters at a constant temperature $T = 20°C$ after $t = 24$ h. The contact force was measured on a split-shaft measuring device. In the FEM calculations the Viton-rubber material behaviour was approximated using the constitutive equations of Mooney–Rivlin[8,9]. In this material model the incompressible non-linear rubber material behaviour is described by the constants $C1$ and $C2$, which are determined by fits to the experimental data from high-precision isothermal uniaxial stress relaxation tests on the Viton-rubber specimen. Considering the complexity of the problem (physically non-linear, geometrically non-linear and non-linear boundary conditions), the correspondence between the measured and calculated results is remarkably good.

The glassfibre test rig

Using the test rig shown in Fig 5 the under-lip contact area was studied. The rig consists of a seal rotating on a fixed hollow steel shaft. A square bundle (1.7 × 1.7 mm) of 50 000 square step-index multi-mode glassfibres each measuring 7.5 × 7.5 μm was manipulated into the steel hollow shaft. Via the glassfibres under-lip video registrations were made through a microscope. Compared with the test rigs used in other investigations of the contact area using a rotating transparent thin hollow perspex shaft via a mirror and microscope, the present test rig has some important advantages.

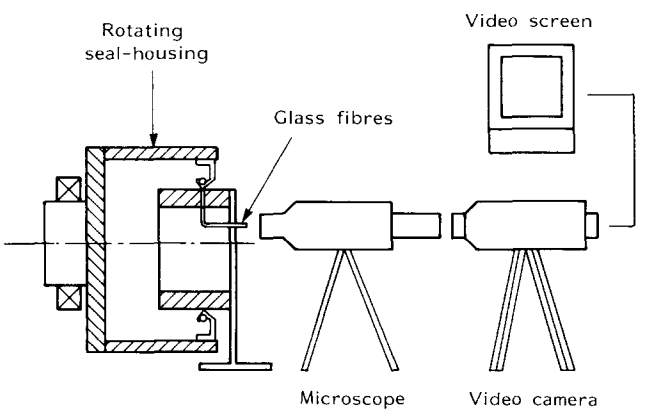

Fig 5 Glassfibre test rig used to study the under-lip contact area

1) The contact conditions such as shaft roughness and wetting angle for oil–steel are only changed in a small region (0.7%) of the circumference of the shaft, where the seal is not running on the shaft surface but on the end of the glassfibre bundle which was given the same radius as the shaft surface.

2) The thermal boundary conditions, ie the heat transfer properties of the shaft, are hardly influenced by the small glassfibre bundle. Compared with a hollow shaft of steel, a hollow shaft of perspex has not only inferior heat transfer properties due to a lower thermal conductivity ($\lambda_{steel}/\lambda_{perspex} = 52/0.19 = 274$), but also due to the fact that the perspex has to be very thin to prevent optical distortion.

An important disadvantage of the glassfibre test rig is that the seal rotates and the shaft is fixed, whereas in most practical situations the shaft rotates and the seal is fixed. To study the influence of centrifugal forces on the contact conditions in the case of a rotating seal, FEM calculations were performed taking into account these centrifugal forces. Fig 6 shows that the influence of centrifugal forces on the contact force becomes important for higher angular velocities.

Observations in the contact area

Fig 7 shows a sketch of the contact zone. The experimental observations made with the glassfibre test rig are summarized as follows

1) Starting with seal angular velocity $\omega_2 = 0$, a gradual increase in ω_2 results in a simultaneous decrease in l_1, l_2 and l_3. Reducing ω_2 to $\omega_2 = 0$ again increases l_1, l_2 and l_3 to their starting values.

2) For a certain set of operating conditions (ω_2, η, T), a steady-state situation occurs in which l_1, l_2 and l_3 remain constant.

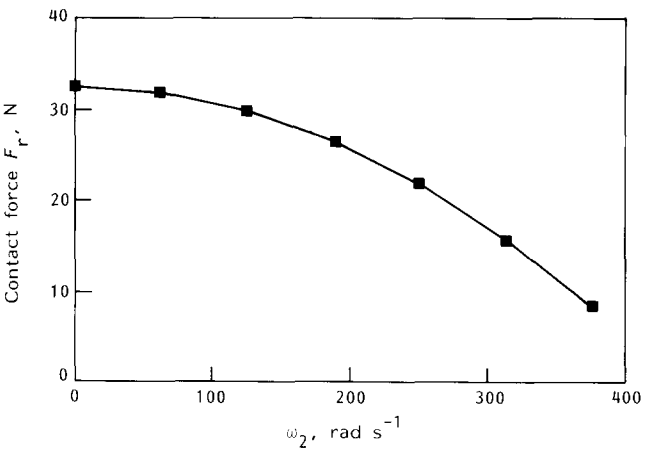

Fig 6 Contact force F_r *under the influence of centrifugal forces as a function of the seal angular velocity* ω_2, *calculated with the FEM, for:* $d_1 = .07$ *m*, T = *20.0°C*, t = *24 h*, ρ_{seal} *(Viton)* = *1.46* × 10^3 *kg* m^{-3}, $m_{spr} = 2.84 \times 10^{-3}$ *kg*

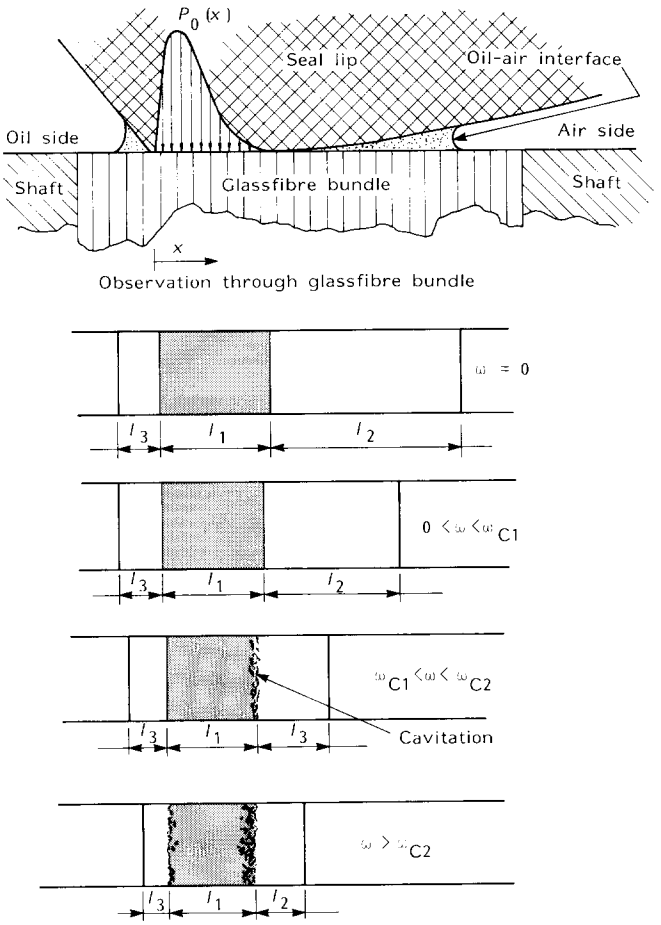

Fig 7 Sketch of the contact zone

3) For $\omega_2 > \omega_{c1}$ cavitation occurs in a small region on the air side of the contact area (Fig 7). For $\omega_2 > \omega_{c2}$ a second cavitation region occurs on the oil side. The intensity of the cavitation and the width of the cavitation regions increases as ω_2 is increased further. In the present case $\omega_{c1} \approx 60$ rad s^{-1} (573 rpm) and $\omega_{c2} \approx 95$ rad s^{-1} (907 rpm).
4) The oil–air interface on the oil side is unstable and oscillates in the axial direction during shaft rotation.

Throughout the experiments no detectable leakage from the oil to the air side of the seal was found. There was no pressure difference between the oil and the air side of the seal.

Discussion

1) The decrease in l_2 with increasing ω_2 can be explained by the pumping action of the seal[1]. The seal pumps the oil from the air side to the oil side. A decrease in l_2 results in increased capillary suction forces. As l_2 decreases, the height $h(x)$ between the shaft and seal surfaces becomes smaller and the radius of the oil–air interface decreases, resulting in an increased pressure drop over the oil–air interface, or, in other words, an increase of the capillary forces.
2) In the steady-state situation the pumping action of the seal is counterbalanced by the capillary forces. These capillary forces are determined by the wetting angles, the surface tension and the gap height.
3) Cavitation can be caused by pressure drops in the valleys of microasperities on the seal or shaft surfaces[7]. Cavitation occurs at both edges of the contact area because here the average oil pressure is lower than in the middle of the contact area. The occurrence of cavitation also depends on local temperatures and on the local shape of the microroughness of the surfaces.
4) On those locations where the bulk oil is not directly in contact with the seal, an (unstable) oil–air interface also can be formed on the oil side of the seal.

Recent work on radial lip seals has concentrated on the pumping mechanism. Often it is assumed that a good seal is a seal which has a high pumping rate. This assumption should be considered with great care. A good seal is a seal with a high sealing performance, and a long service life. A very high pumping rate may lead to a condition of starved lubrication resulting in wear of the seal contact area and premature failure. Further care should be taken when studying the pumping effect experimentally by injecting oil in the gap between seal and shaft on the air side of the seal. Then a transient situation is created which does not correspond to the normal steady-state running conditions. Directly after the injection, the pressure drop over the oil–air interface is reduced due to a sudden increase in l_2. The influence of this effect on the pumping action is not clear yet, but it can be concluded that it does influence the lubrication conditions from the considerable decrease in torque, measured during the pumping action (see Refs 1 and 3). This article therefore attempts to determine the pumping action for a steady-state situation by calculating the pressure drop over the oil–air interface.

Drop in pressure over the oil–air interface

On the air side there is a drop in pressure over the oil–air interface. The pressure drop can be expressed as

$$\Delta p = \gamma / R \qquad (1)$$

where γ is the surface tension of the oil and R is the radius of the interface. In the present case R is determined by the distance x, the gap height $h(x)$ and the wetting angles α_1 for oil–rubber and α_2 for oil–steel; thus $R = R(x, h(x),$

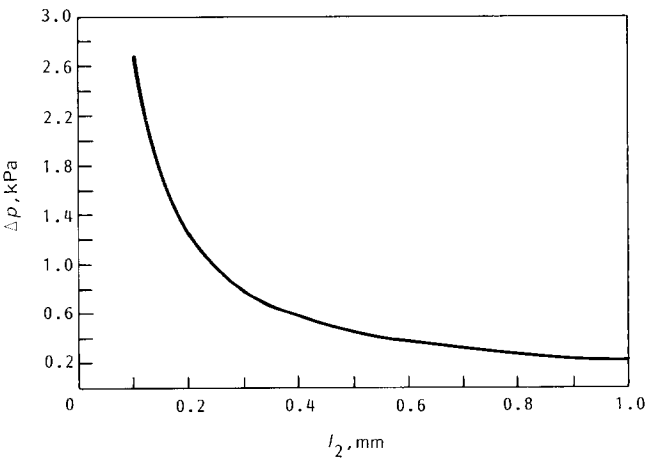

Fig 8 Calculated pressure drop over oil–air interface as a function of the distance between the oil–air interface on the air side and the contact area, $\Delta p = \Delta p(l_2)$

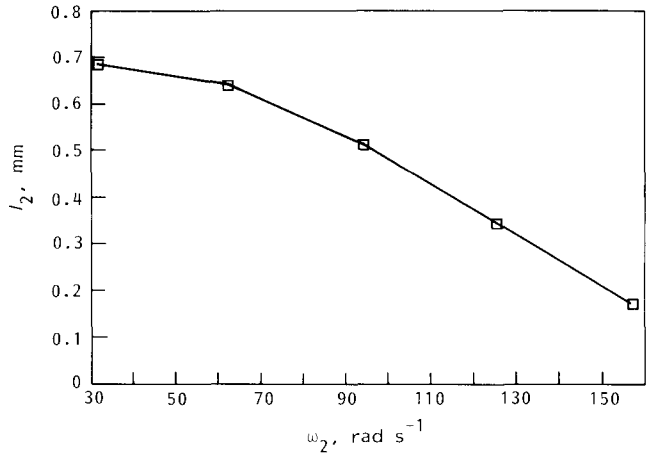

Fig 9 The distance from the oil–air interface on the air side to the contact area as a function of the seal angular velocity, $l_2 = l_2(\omega_2)$, measured using the glassfibre test rig

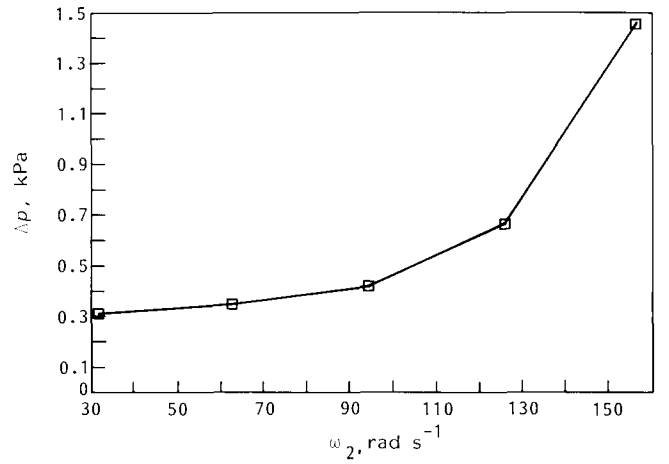

Fig 10 Calculated pressure drop over oil–air interface as a function of the angular velocity $\Delta p = \Delta p(\omega_2)$, calculated with the measured data $l_2 = l_2(\omega_2)$

α_1, α_2). R can be calculated by solving equation (A8) in the appendix.

Fig 8 shows the calculated pressure drop over the oil–air interface as a function of l_2. The function $h(x)$ was determined from the deformed seal contour, calculated using the FEM method.

To study the pumping action of the seal $l_2 = l_2(\omega_2)$ was determined experimentally using the glassfibre test rig (Fig 9). With these data and Eq (1) the pumping pressure $\Delta p = \Delta p(\omega_2)$ was calculated (Fig 10).

Conclusions

1) The contact conditions governing the sealing mechanism are influenced by temperature.
2) Finite element calculations can provide reliable information on these contact conditions.
3) In a steady-state situation the pumping action of the seal is counterbalanced by the capillary forces of the oil–air interface on the air side.
4) Cavitation occurs first on outer edges of the contact area.

To obtain a better understanding of seals there is a strong need for a physical model which describes the sealing mechanism, taking into account the pumping effect, capillary forces, cavitation and the influence of temperature.

Acknowledgement

The author would like to thank the Freudenberg Company in Weinheim, Germany, for providing test seals and the Viton-rubber specimen for the material characterization tests.

References

1. **Kammüller M.** Zur Abdichtwirkung von Radial-Wellendichtringen. *Thesis, 1986, University of Stuttgart, FRG* (in German)
2. **Rajakovics G.** Beitrag zur kenntnis der Wirkungsweise von Berührungsdichtungen. *Dissertation, Wein, 1970* (in German)
3. **Müller H.K.** Concepts of sealing mechanism of rubber lip type rotary shaft seals. *Proc. 11th Conf. on Fluid Sealing, BHRA, 1987, paper K1, 698–709*
4. **Horve L.A.** A macroscopic view of the sealing phenomenon for radial lip oil seals. *Proc. 11th Conf. on Fluid Sealing, BHRA, 1987, paper K2, 710–731*
5. **Nakamura K.** Sealing mechanism of rotary shaft lip type seals. *Tribology Int., April 1987,* **20** (2), *90–101*
6. **Adam N.K.** *The Physics and Chemistry of Surfaces. Dover Publications, New York, 1968*
7. **Hamilton D.B., Walowit J.A. and Allen C.M.** Microasperity lubrication. *J. Basic Engng, 1968, 351–355*
8. **Hibbit, Karlson and Sorensen** *ABAQUS FEM Software, Users Manuals (version 4–5)*
9. **Treolar L.R.G.** *The Physics of Rubber Elasticity. Clarendon Press, Oxford, 1975*

Appendix. Calculation of the pressure drop over the interface

The formation of an oil–air interface and the occurrence of a pressure drop Δp over an oil–air interface can be explained physically in terms of minimalization of the system's energy. For the physical background the reader is referred to Ref 6. This appendix is restricted to calculation of the pressure drop Δp over the oil–air interface on the air side of the seal when the location of the oil–air interface, ie the x coordinate of the oil–air interface, is known (Fig 11). The following assumptions and simplifications have been made.

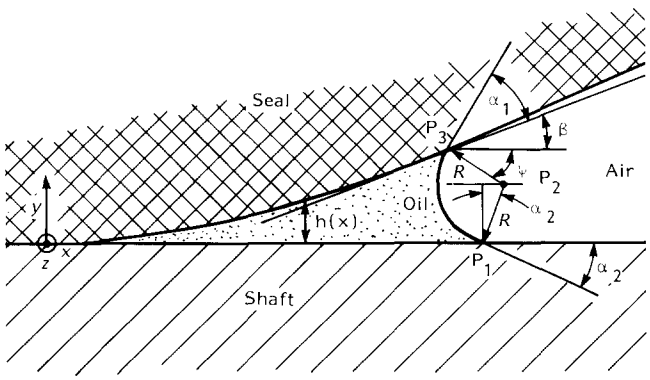

Fig 11 Sketch of the oil–air interface on the air side of the seal

1) In the xy plane, the oil–air interface has a constant curvature $1/R_{xy} = 1/R$. The curvature $1/R_{xz}$ in the xz plane is small and can be neglected compared with $1/R_{xy}$.
2) The influence of temperature on γ, α_1 and α_2 is neglected.
3) The influence of velocity on γ, α_1 and α_2 is neglected.
4) The influence of centrifugal forces and gravitational forces on the curvature R of the oil–air interface is neglected.

Based on these assumptions the calculation of Δp is relatively simple. For the coordinates (x_2, y_2) of the centre point P_2 of the oil–air interface:

$$x_2 = x_1 + R\sin\alpha_2 \tag{A1}$$

$$y_2 = R\cos\alpha_2 \tag{A2}$$

where x_1 is the x coordinate of the point P_1.

The coordinates (x_3, y_3) of point P_3, where the oil–air interface is in contact with the seal surface, can be written, using Eqs (A1) and (A2):

$$x_3 = x_2 - R\cos\psi = x_1 + R(\sin\alpha_2 - \cos\psi) \tag{A3}$$

$$y_3 = y_2 + R\sin\psi = R(\cos\alpha_2 + \sin\psi) \tag{A4}$$

where

$$\psi = \pi/2 - (\alpha_1 + \beta) \tag{A5}$$

$$\beta = \arctan\left(\left.\frac{dh}{dx}\right|_{x_3}\right) \tag{A6}$$

Using Eq (A4) yields:

$$h(x_3) = y_3 = R(cos\alpha_2 + \sin\psi) \tag{A7}$$

or

$$h(x_3) = R(x_1)(\cos\alpha_2 + \sin\left[\alpha_1 + \arctan\left(\left.\frac{dh}{dx}\right|_{x_3}\right)\right] \tag{A8a}$$

where

$$x_3 = x_1 + R(x_1)\left(\sin\alpha_2 - \sin\left[\alpha_1 + \arctan\left(\left.\frac{dh}{dx}\right|_{x_3}\right)\right]\right) \tag{A8b}$$

For a certain value x_1, the radius $R = R(x_1)$ of the oil–air interface can now be determined from Eqs (A8a) and (A8b) using a numerical root finding algorithm, eg a Newton–Raphson scheme. The pressure drop $\Delta p(x_1)$ can now be calculated using

$$\Delta p(x_1) = \gamma\left(\frac{1}{R_{xy}} + \frac{1}{R_{xz}}\right) \approx \frac{\gamma}{R_{xy}} = \frac{\gamma}{R(x_1)} \tag{A9}$$

The wetting angles α_1 and α_2 can be determined by measuring the contact angle of a droplet of oil on a flat surface of rubber and a droplet of oil on a flat surface of steel. Accurate experimental determination of α_1 and α_2 is difficult however due to hysteresis effects, the influence of surface roughness, and the influence of gravitational forces. Measurement of α_1 holds an extra complication: due to diffusion of oil into the rubber the wetting angle α_1 may change within 30 min from 15° to 30°.

The data represented in Figs 8 and 10 were calculated using the following values:

$\alpha_1 = 0.524$ rad (30°)

$\alpha_2 = 0.122$ rad (7°)

$\gamma = 0.0315\ \mathrm{N\,m^{-1}}$

The experiments were performed using Shell oil Tellus 46.